sustainability

MDPI

Article

Repurposing Quality-Downgraded Fluorinated Carbon Nanotubes as Eco-Additives in Microgel Composites for Sustained Water Release

Favour Lewechi Ezeogu, Gunendra Prasad Ojha, Promise Uzoamaka Otuokere, Mohammad Tarequl Islam, Tony Grady and Yunxiang Gao *

Department of Chemistry and Physics, Prairie View A&M University, Prairie View, TX 77446, USA; potuokere@pvamu.edu (P.U.O.)
* Correspondence: yugao@pvamu.edu

Abstract: While significant efforts have been made to recycle metals like lithium or cobalt for sustainable development in the battery industry, the reuse of other high-value materials, such as fluorinated carbon nanotubes (FCNTs), remains underexplored. This study introduces a novel, eco-friendly method to repurpose quality-downgraded FCNTs (QD-FCNTs) as effective nano-additives in polyacrylamide (PAAm) microgel composites for water retention applications. Because QD-FCNTs are rich in surface defects, by employing a mild surface treatment with a low dosage of organic electron donor *N*,*N*,*N*′,*N*′-tetramethyl-*p*-phenylenediamine, we enhanced the hydrophilicity of QD-FCNTs without additional energy input or a large quantity of harmful chemicals. This treatment significantly improved the interaction between QD-FCNTs and PAAm microgels, leading to a 55% increase in water retention time compared to the composites made of untreated QD-FCNTs. Our findings present a sustainable approach to extending the lifecycle of FCNTs, contributing to the circular economy and offering practical solutions for potential water management in agriculture and environmental technologies.

Keywords: fluorinated carbon nanotubes; polyacrylamide composites; microgels; sustained water release; waste repurposing

check for updates

Citation: Ezeogu, F.L.; Ojha, G.P.; Otuokere, P.U.; Islam, M.T.; Grady, T.; Gao, Y. Repurposing Quality-Downgraded Fluorinated Carbon Nanotubes as Eco-Additives in Microgel Composites for Sustained Water Release. *Sustainability* **2024**, *16*, 9468. https://doi.org/10.3390/su16219468

Academic Editors: Farshid Pahlevani and Smitirupa Biswal

Received: 12 September 2024
Revised: 28 October 2024
Accepted: 29 October 2024
Published: 31 October 2024

Copyright: © 2024 by the authors. Licensee MDPI, Basel, Switzerland. This article is an open access article distributed under the terms and conditions of the Creative Commons Attribution (CC BY) license (https://creativecommons.org/licenses/by/4.0/).

1. Introduction

By repurposing high-value materials at the end of their life cycle, we can extend their utility despite the diminished original functionality from prolonged use. This strategy not only maximizes resource efficiency but also aligns with sustainable practices by giving a second life to materials that would otherwise be discarded. With the global trends of shifting to a more sustainable future, managing and repurposing high-value materials used in energy storage applications becomes particularly challenging [1,2]. Current extensive research in this area has focused on recycling valuable metals like lithium, cobalt, nickel, and manganese [3–5], as well as other materials used such as electrolytes [6,7], cathode [8–10], and anode [11] in spent lithium-ion batteries (LIBs). Despite low-dimensional carbon nanomaterials having shown exceptional electronic properties [12,13] and enabling various high-performance energy storage applications [14,15], the recycling or reuse of these high-value carbon nanomaterials, such as carbon nanotubes (CNTs), remains significantly underexplored [16–18]. Among various value-added carbon nanomaterials, the fluorinated ones [19], especially fluorinated carbon nanotubes (FCNTs), are particularly useful, but energy- and resource-costly [20,21]. FCNTs with extraordinarily high fluorination levels are even prone to quality degradation over time due to defluorination, posing significant barriers to their sustainable applications.

In light of these challenges, we are trying to explore in this work the potential repurposing of quality-downgraded fluorinated carbon nanotubes (QD-FCNTs) to reduce their

overall energy and environmental costs. Considering that various carbon nanomaterials have been employed as innovative nano-additives in functional composites [22], especially via the integration with microgels for environmental, biomedical, energy, and catalysis purposes [23], we propose here an eco-friendly method to re-functionalize QD-FCNTs at a near-zero energy cost to enhance their hydrophilicity and enable their reuse as nano-additives in polyacrylamide (PAAm) microgel composites for extended water retention for potential sustainable agricultural practices.

As a brief background review, fluorinated carbon nanotubes have been extensively studied for their unique properties and applications in the renewable energy and storage sectors. For example, in supercapacitor applications, FCNTs demonstrate enhanced performance compared to non-fluorinated counterparts, with improvements in specific capacitance, rate capability, and cycling stability [20]. Additionally, FCNTs are used in silicon heterojunction solar cells [24], perovskite solar cells [25], various batteries [26], catalysts [27,28], and reinforced composites [29]. These applications benefit from the partial fluorination of CNTs, which balances conductivity and functionality, leading to superior electrochemical properties. Lithium and sodium primary batteries using FCNTs with an optimal fluorine-to-carbon ratio as the cathode materials have achieved both high energy density (1147 $Wh \cdot kg^{-1}$) and power density (8998 $W \cdot kg^{-1}$), outperforming conventional carbon–fluoride materials [30,31]. Further studies also confirmed that the selective fluorination of the outer nanotube layers preserves electronic conductivity while enhancing the performance of primary lithium batteries [32].

Beyond energy storage, FCNTs play a critical role as efficient electrocatalysts. In the efforts of converting CO_2 and nitrate to urea under ambient conditions, FCNTs offer higher urea yields and enhanced electro-catalytic efficiency [33]. They can also modulate the electron configuration of metalloporphyrin-like active sites to reduce the energy barrier for CO_2 reduction [34]. In fuel cells, FCNTs enhance the oxygen reduction reaction (ORR) by providing a higher density of active sites [35]. Moreover, FCNTs can serve as valuable reinforcing fillers in polymer composites [36].

Despite FCNT's superior performance in diverse applications, our previous research has shown that the stability of fluorine content on the strained nanotube surfaces decreases as the carbon lattice curvature increases [37,38]. Fluorinated nanolattice of extremely high curvature strain, such as that of the fluorinated single-walled carbon nanotubes (FSWNTs), are prone to defluorination under mild chemical conditions or even after prolonged storage. Such quality down-gradation further drives up the cost of widely utilizing the high-value FCNTs. On the other hand, QD-FCNTs obtained from long-term degradation, despite losing their original functionality, potentially have rich surface defects that facilitate the re-functionalization of QD-FCNTs, as repurposing CNTs often requires specific surface treatments. The conventional methods used for CNT re-functionalization typically involve energy-intensive processes and rely on using large quantities of environmentally harmful chemicals, such as heated concentrated nitric acid or piranha solution bath [39]. Compared to pristine CNTs, QD-FCNT's rich defects [40] could potentially be leveraged for much milder CNT re-functionalization, making them a better candidate for eco-friendly processing and reusing of CNTs for other sustainable technology applications.

As for agricultural practices, one potential contribution CNTs could make is to serve as nano-additives in hydrogels for water retention with enhanced mechanical properties. However, conventional hydrogels are macroscopic 3D polymer networks capable of retaining 500–600 times their own weight in water. Such highwater uptake can cause significant volume changes in soil (both via swelling and shrinkage), negatively affecting plant development. Moreover, their extraordinarily strong water absorption capability can compete with roots for water. Microgels, while absorbing less water than hydrogels, still retain tens of times their own weight in water, enhancing soil moisture without causing excessive swelling. Additionally, their large surface area facilitates faster fertilizer absorption and more efficient moisture uptake in a short time. Despite these advantages, however, microgels are soft, micron-sized colloidal particles that can easily run off in soil. In this work,

by incorporating QD-FCNTs with PAAm microgels, we aim to create composites that not only improve water retention but also offer nano-additive assisted microgel flocculation to improve the stability of microgels, thereby potentially benefiting their application in sustainable agricultural practices.

Taking advantage of the above-mentioned rich defects on QD-FCNTs, we showcase a nearly zero-energy re-functionalization method for QD-FCNTs to improve their interaction with hydrophilic PAAm microgels and reuse them as nano-additives in the formed QD-FCNT/PAAm microgel composites for elongated water retention. As illustrated in Scheme 1, at room temperature, a small amount of strong organic electron donor *N*,*N*,*N*′,*N*′-tetramethyl-*p*-phenylenediamine (TMPD) was used to treat the defects on the QD-FCNTs surface, resulting in a more stable composite material with improved water retention capabilities. Such a mild surface treatment process avoids high energy consumption and the usage of large quantities of environmentally harmful chemicals, which not only extends the lifecycle of the high-value FCNTs but also aligns well with the principles of the circular economy by minimizing waste and reducing environmental impacts.

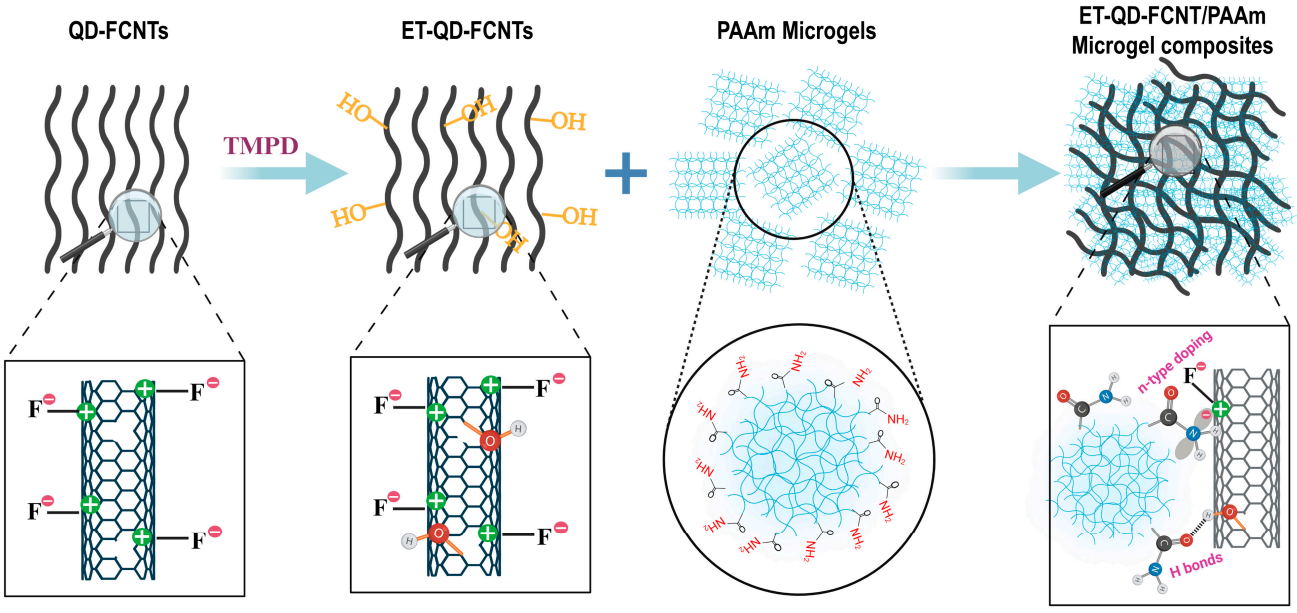

Scheme 1. Schematic illustration showing the treatment of QD-FCNTs with *N*,*N*,*N*′,*N*′-tetramethyl-*p*-phenylenediamine (TMPD) to enhance their hydrophilicity for improving interaction with PAAm microgels.

2. Experimental

2.1. Materials and Chemicals

The free radical initiator 2,2′-azobis(2-methylpropionitrile) (M.W.: 164.21 g/mol, purity: 98+%) was purchased from Sigma-Aldrich (Burlington, MA, USA) and stored in a refrigerated environment until use. The crosslinker *N*,*N*′-methylene-*bis*-acrylamide (M.W.: 154.17 g/mol, chemical formula: $C_7H_{10}N_2O_2$, purity: 98+%), acrylamide monomer (M.W.: 71.08 g/mol, chemical formula: C_3H_5NO, purity: 98+%), and the organic electron donor *N*,*N*,*N*′,*N*′-tetramethyl-*p*-phenylenediamine (TMPD; M.W.: 164.25 g/mol, Purity: 98+%) were obtained from Alfa Aesar (Ward Hill, MA, USA). Denatured ethyl alcohol was purchased from NCL Placentia (M.W.: 46.068 g/mol, chemical formula: C_2H_5OH, purity: 99.5%, 200 proof). Fluorinated single-walled carbon nanotubes were acquired from Nanoshel, Inc. (Congleton, UK), and stored at room temperature in the air for over 1.5 years. The long-term storage led to significant degradation in fluorine content, and these nanotubes are referred to as QD-FCNTs (quality-downgraded FCNTs) in this study.

2.2. PAAm Microgel Synthesis

Polyacrylamide microgel was synthesized in an alcoholic environment. Briefly, 1.00 g of *2,2′*-azobis(2-methylpropionitrile), 216 mL of 99.5% ethyl alcohol, 1.17 g of *N,N′*-methylene-*bis*-acrylamide, and 43.2 g of acrylamide monomer were used. The acrylamide monomer was dissolved in ethanol with thorough stirring to ensure complete dissolution. The crosslinker, *N,N′*-methylene-*bis*-acrylamide, was then added and stirred on an electromagnetic stirring plate until homogeneity was achieved. Finally, the free radical initiator *2,2′*-azobis(2-methylpropionitrile) was introduced into the solution and stirred uniformly. The mixture was purged with argon gas for 30 min to remove dissolved oxygen. Polymerization was carried out by heating the solution in a pre-heated water bath at 60 °C for 18 h. Upon completion of the reaction, the obtained microgel product was dried in an oven at 50 °C for 72 h.

2.3. Carbon Nanotubes Surface Treatment

For the surface treatment of QD-FCNTs, 80 mg of TMPD was dissolved in 30 mL of ethanol using a bath ultrasonicator for 20 min to ensure complete dispersion. Next, 200 mg of QD-FCNTs were added, followed by probe sonication for another 20 min to achieve uniform dispersion. The mixture was then covered and left undisturbed at room temperature for 16 h to promote thorough interaction between the TMPD molecules and QD-FCNTs. The TMPD-treated QD-FCNTs solution was then vacuum-filtered through a 0.1 μm PTFE membrane (Deschem, Changshu, China) to collect the surface-treated nanotubes. The collected film was rinsed with ethanol three times and dried in an oven at 50 °C to remove residual solvent, preparing it for further characterization. Control samples involving QD-FCNTs without TMPD treatment went through the same solution processing procedure without adding TMPD.

2.4. Preparation of QD-FCNTs/PAAm Microgel Composites

To prepare QD-FCNTs/PAAm microgel composites, 1.44 g of dried PAAm microgel was dispersed in 30 mL of D.I. water and subjected to sonication using a 360 W ultrasonic homogenizer for 10 min. Then, 72 mg of QD-FCNTs were added, and the mixture was sonicated at 360 W for another 20 min to achieve a stable, well-dispersed liquid composite of QD-FCNTs/PAAm-microgel. The formed composites were then centrifuged using a VWR International (Darmstadt, Germany) small benchtop Medifuge centrifuge machine at 6000 rpm. The supernatant of the centrifuged solution was carefully decanted and the QD-FCNTs/PAAm microgels collected at the tip area of the centrifuge tubes were used for further study.

2.5. Instruments and Characterization

Scanning electron microscopy (SEM) was conducted using an FEI Quanta 400 ESEM (InTouchScope software, Version 1.11) with a secondary electron detector at an accelerating voltage of 5 kV. Energy dispersive X-ray spectroscopy (EDX) elemental analysis was performed using a JEOL JSM-6010LA (Tustin, CA, USA) instrument operated through InTouchScope software (Version 1.11) at 7 kV. Raman spectra were recorded using a Thermo Fisher DXR3 Raman spectrometer (Madison, WI, USA) with a 785 nm laser of 1 mW power. Thermogravimetric analysis (TGA) was carried out on a TA Instruments TGA 2050 system at a heating rate of 10 °C/min in air. Infrared spectra were collected using a Thermo Scientific iD7 ATR accessory with an FT-IR spectrometer. The size of the microgel was measured using Anton Paar's dynamic light scattering instrument Litesizer DLS 700 (Houston, TX, USA).

2.6. Water Retention Study

The water retention studies of the QD-FCNT/PAAm microgel composites, both with and without TMPD treatment, were evaluated by monitoring the rate of water loss over time under controlled conditions. The prepared composites collected in the centrifuge tubes were

placed inside a 35 °C incubator with a vent to simulate conditions of warm temperatures in agricultural fields, which has accelerated water evaporation. The sample was periodically weighed at certain time intervals to track the reduction in water content. The initial weight of the composite (fully hydrated) was recorded, and subsequent measurements were taken until a constant weight was reached, indicating complete water evaporation. The percentage of retained water at each time point was calculated based on the initial mass of the composites.

3. Results and Discussions

Fluorinated carbon nanotubes can experience significant defluorination under mild conditions, depending on their fluorination method [40] and the curvature strain on the C-F bonds [37]. In this work, we used a type of FSWNT with an initial fluorine content of above 50% by mass, as provided by the manufacturer. We found that at this high fluorination level, FSWNTs can lose nearly all their fluorine content after long-term storage at room temperature. As shown in Table 1, after 1.5 years of storage at room temperature, the fluorine content had dramatically decreased to approximately 1.5%. According to Mickelson et al., the maximum C ratio for FSWNTs that can be achieved through non-invasive fluorination is 2:1, which corresponds to a fluorine fraction of 44% by mass. Although higher fluorination levels can be attained, they begin to damage the carbon nanotube backbone with further increased fluorination contents [41]. Therefore, it is reasonable to expect that these highly fluorinated CNTs are more susceptible to mild degradation conditions due to the high defect levels. Once the fluorine atoms are removed over long-term use or storage, some of the exposed carbon sites will remain as bare carbon defect sites.

As addressed earlier, re-functionalization is often necessary to restore the properties of CNTs for reuse. Since defect sites are generally more reactive and can undergo chemical modifications under milder conditions [42,43], we hypothesize that QD-FCNTs with more defluorination-induced defects can be functionalized under eco-friendly conditions.

To improve the hydrophilicity of CNTs for better interaction with microgels, introducing hydrophilic hydroxyl (-OH) or carbonyl (-C=O) groups to the sidewalls of CNTs is a well-known strategy [44]. However, conventional methods for introducing hydroxyl groups to the CNT surface typically require energy-intensive processes and large amounts of environmentally harmful chemicals, such as concentrated nitric acid or piranha batch solutions [39]. Even though some studies employ more efficient heating methods like microwaves, these still consume extra energy and substantial quantities of acids [45]. Given that defluorination of QD-FCNTs often leaves surface defects on the nanotube lattice [40], we propose a novel approach to treating these defect-containing QD-FCNTs using *N*,*N*,*N*′,*N*′-tetramethyl-*p*-phenylenediamine (TMPD), a strong organic electron donor. By performing this treatment at room temperature without additional energy input, we successfully enhanced the hydrophilicity of the QD-FCNTs and their interactions with PAAm microgels. Due to their polarity and slight water solubility, TMPD molecules can be used in small amounts in polar solvents for CNT surface treatments, reducing environmental impact. Rather than soaking the CNTs in bulk quantities of strong acids, we add milligram-level amounts of TMPD and treat the QD-FCNTs overnight at room temperature. Owing to its lower environmental and energy footprint—and for brevity—we refer to the TMPD-treated QD-FCNTs as Eco-friendly Treated QD-FCNTs (ET-QD-FCNTs) in this paper.

Figure 1 shows SEM images and EDX elemental analysis of the QD-FCNTs before and after TMPD treatment and ET-QD-FCNTs/PAAm composites. Both the untreated QD-FCNT control sample (Figure 1(A_1)) and the TMPD-treated ET-QD-FCNTs sample (Figure 1(B_1)) exhibit compact nanotube networks composed of FCNT bundles, with observed bundle lengths of up to 80 μm. The similarity in CNT length and morphology before and after TMPD treatment indicates that the CNT structure is well-preserved due to the mildness of the treatment. EDX elemental analysis (Figure 1(A_2,B_2)) shows a slight increase in oxygen content after TMPD treatment. As listed in Table 1, the fluorine content

decreased by only 0.2%, indicating that the remaining fluorine content after long-term storage is relatively stable. An oxygen content of 6.02% was observed in the QD-FCNTs because of the long-term storage in air, during which some defect sites on QD-FCNTs may react with environmental oxygen-containing species such as moisture and oxygen. After treatment with TMPD, the observed further increase in oxygen content, though small, is notably higher than the decrease in fluorine content, suggesting that additional oxygen was bonded to the nanotubes due to the TMPD treatment. This is further supported by the water contact angle change of thin films prepared from QD-FCNTs (Table 1), which decreased from 150° (untreated) to 120° after TMPD treatment, indicating that even a slight increase in oxygen content via such an eco-friendly re-functionalization can significantly improve the hydrophilicity of the CNTs surface, which further enhance CNT's interaction with the more hydrophilic PAAm microgels.

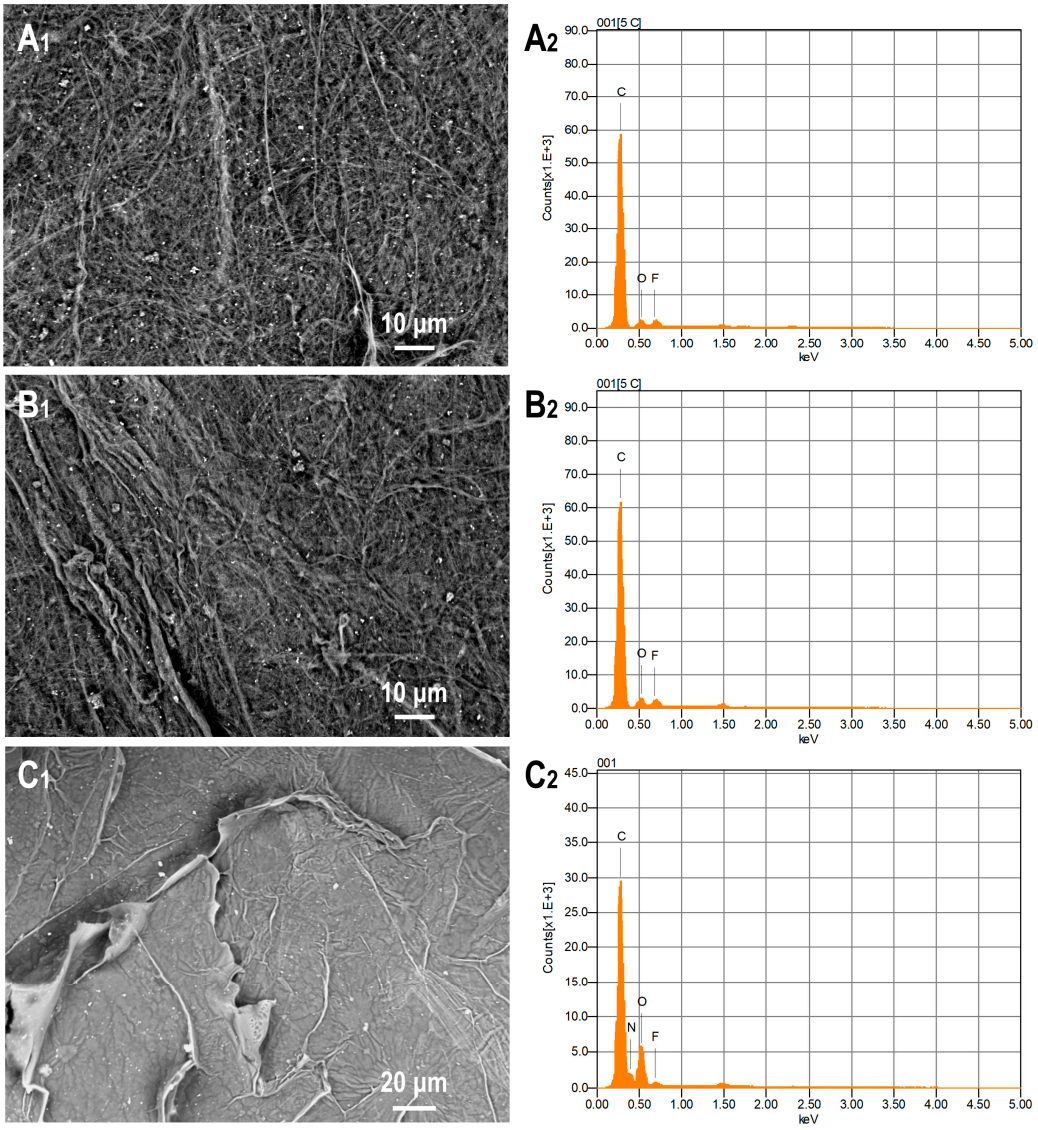

Figure 1. SEM images (**A$_1$**–**C$_1$**) and EDX elemental analysis (**A$_2$**–**C$_2$**) of QD-FCNTs (**A$_1$**,**A$_2$**), ET-QD-FCNTs (**B$_1$**,**B$_2$**), and ET-QD-FCNTs/PAAm composites (**C$_1$**,**C$_2$**).

Figure 1(C$_1$) displays the SEM image of the ET-QD-FCNTs/PAAm microgel composites. The image reveals that the QD-FCNTs are homogeneously coated with PAAm microgels. The characteristic nanotube bundles of the ET-QD-FCNTs are no longer visible because the bulkier PAAm microgels are uniformly distributed over the CNT surface, likely due to hydrogen bonding and/or physical attractions between the functional groups

present on both components (Scheme 1). Figure 1(C_2) shows the corresponding elemental analysis of the ET-QD-FCNTs/PAAm microgel composites shown in Figure 1(C_1), highlighting the appearance of nitrogen signals and an increase in oxygen signals attributable to the presence of PAAm microgels.

Table 1. EDX and Contract Angle Analysis of QD-FCNTs and ET-QD-FCNTs.

Elements and Contacting Angle	QD-FCNTs	ET-QD-FCNTs
Carbon, mass%	92.42	91.85
Oxygen, mass%	6.02	6.79
Fluorine, mass%	1.56	1.36
Film Contacting Angle	150°	120°

To further investigate the surface chemical changes caused by the TMPD treatment, we collected ATR-FTIR spectra of the QD-FCNTs (Figure 2A) [46]. The untreated QD-FCNTs show a small peak at 1210 cm^{-1}, corresponding to the C-F bond stretching vibration, with no other significant peaks. After TMPD treatment, no peak related to the surface adsorption or chemical bonding of TMPD molecules was observed. Instead, a notable peak corresponding to -OH stretching emerged at 3333 cm^{-1} [47], consistent with the increased oxygen content observed in the EDX analysis. This suggests the formation of hydrophilic hydroxyl groups on the CNT surface, likely due to TMPD's role in generating reactive species (e.g., TMPD$\bullet^{+}$ radical cations). Forming these radicals donates electrons to CNT defect sites for further reacting with water, leading to the formation of hydroxyl groups at defect sites. Simultaneously, multiple peaks appeared between 2900 and 3100 cm^{-1}, which can be assigned to the C-H stretching vibration bonds on some reduced defect sites.

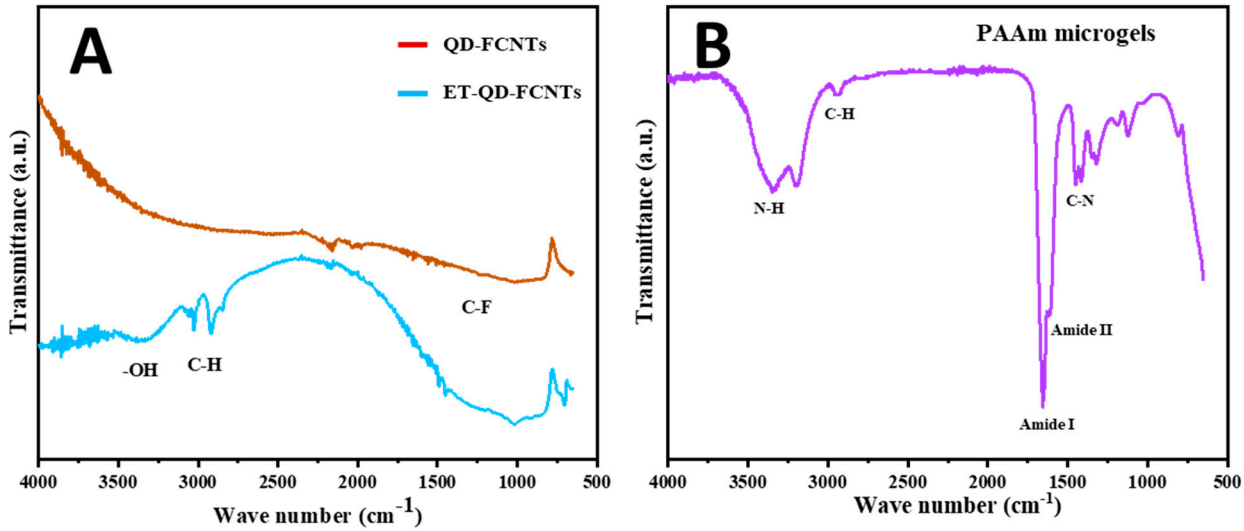

Figure 2. ATR-FTIR spectra of (**A**) QD-FCNTs and ET-QD-FCNTs and (**B**) pure PAAm microgels.

The formation of hydroxyl groups at defect sites proved by the FT-IR characterization increases the polarity of the CNT surface, improving its affinity for water and other polar molecules. The increased hydrophilicity facilitates stronger interactions with the hydrophilic PAAm microgels through hydrogen bonding and dipole–dipole interactions, which may contribute to the homogeneous distribution of PAAm microgels on the CNT surface, leading to improved composite stability.

Raman spectroscopy is a powerful tool for characterizing various carbon allotropes by analyzing the rotational and vibrational spectral signatures of carbon atoms within their lattice structures [48]. In this study, we used Raman spectroscopy with a 1 mW, 785 nm laser to investigate both QD-FCNTs and ET-QD-FCNTs. Typically, Raman spectra of SWNTs exhibit three key bands: the Radial Breathing Mode (RBM) bands, D-band, and G-band.

The RBM band, observed in the low-frequency range (100–300 cm^{-1}), is related to nanotube diameter and provides insights into their size and chirality. The D-band, centered around 1300 cm^{-1}, indicates defects and disorder within the carbon lattice, with higher intensity reflecting a greater presence of sp^3-hybridized (diamond-like) carbon atoms. The G-band, near 1590 cm^{-1}, corresponds to the tangential stretching mode of carbon–carbon bonds in the sp^2-hybridized graphene-like lattice of CNTs [49].

Our Raman analysis revealed that the untreated QD-FCNTs samples displayed the typical spectral features of SWNTs, with a strong G-band at 1591.2 cm^{-1} and a weak D-band at 1301.8 cm^{-1} (Figure 3A). The low D-band intensity supports the significant loss of fluorine from the FCNTs and partial recovery toward pristine CNTs. After the eco-friendly TMPD-treatment, the ET-QD-FCNTs kept the same G-band intensity as that of the untreated QD-FCNTs (Figure 3B); however, the amplified D-bands shown in Figure 3C demonstrated that the intensity of the disorder-representing D-band of the ET-QD-FCNTs increased compared to the untreated QD-FCNTs, which agrees with the FT-IR analysis in Figure 2A and EDX analysis in Table 1. The G-band in Figure 3B has a downshifted shoulder of around 1570 cm^{-1}. In fact, the G-band can be split into two sub-peaks called the G^+ peak and the G^- peak [50]. G^+ peak originates from LO (longitudinal optical) phonons, which involves vibrations where the carbon atoms move parallel to the axis of the nanotubes, whereas G^- peak originates from TO (transverse optical) phonons and involves vibrations where the carbon atoms move perpendicular to the axis of the nanotube. The increase of G^- peak after TMPD treatment (ET-QD-FCNTs in Figure 3B) compared to that of the untreated (QD-FCNTs in Figure 3B) is due to the treatment-caused hydroxyl functionalization, which introduced more sp^3 hybridization and increased disorder in the carbon lattice, enhancing the transverse optical phonon modes. Such hydroxyl functionalization also caused a downshift of the G^- band from 1570.6 to 1568.8 cm^{-1} due to the weakening of the carbon–carbon bonds near the functionalized sites.

Additional evidence was found in the RBM region (100–300 cm^{-1}), which is characteristic of radial vibrations in perfectly cylindrical nanotubes. The RBM band frequency of SWNTs (ω_{RBM}) is inversely proportional to their diameter (d_t), following the relation $\omega_{RBM} = 248/d_t$ [51]. In Figure 3D, the RBM peaks at 153.3, 205.1, and 263.8 cm^{-1} correspond to nanotube diameters of 1.62 nm, 1.21 nm, and 0.94 nm, respectively. According to the Kataura plot, which relates SWNT diameter to electronic properties and chirality [52], under 785 nm laser excitation (1.58 eV), RBM peaks below 162 cm^{-1} ($d_t > 1.53$ nm) indicate metallic nanotubes, while those above 200 cm^{-1} ($d_t < 1.24$ nm) are from semiconducting tubes. Fluorination generally disrupts the cylindrical structure of SWNTs by introducing sp^3 hybridization, causing the RBM bands to disappear, but they can reappear when defluorination occurs [53]. In this study of QD-FCNTs, the reappearance of the prominent RBM band at 153.3 cm^{-1} after long-term storage suggests a substantial recovery of metallic SWNTs, while the weaker RBM bands at 205.1 cm^{-1} and 263.8 cm^{-1} indicate less recovery of pristine semiconducting SWNTs, despite significant defluorination. Since as-synthesized SWNTs typically consist of approximately 2/3 semiconducting and 1/3 metallic nanotubes and achieving perfect chirality control is difficult due to the similar structures and formation energies of the two types [54], the dominant intensity of metallic SWNT RBM bands over semiconducting ones suggests that metallic tubes are more favorably recovered during the long-term natural defluorination. The discrepancy in recovery between metallic and semiconducting nanotubes can be attributed to their differing electronic structures. Metallic CNTs have delocalized π electrons across their lattice, which tend to preserve nanotube integrity. In contrast, semiconducting CNTs have a more localized electron density and a bandgap, making them more vulnerable to reactions with species such as OH free radicals [55]. Thus, the RBM bands from the semiconducting nanotubes may be continuously suppressed due to reactions with reactive species in the environment during the quality downgrading process of FSWNTs.

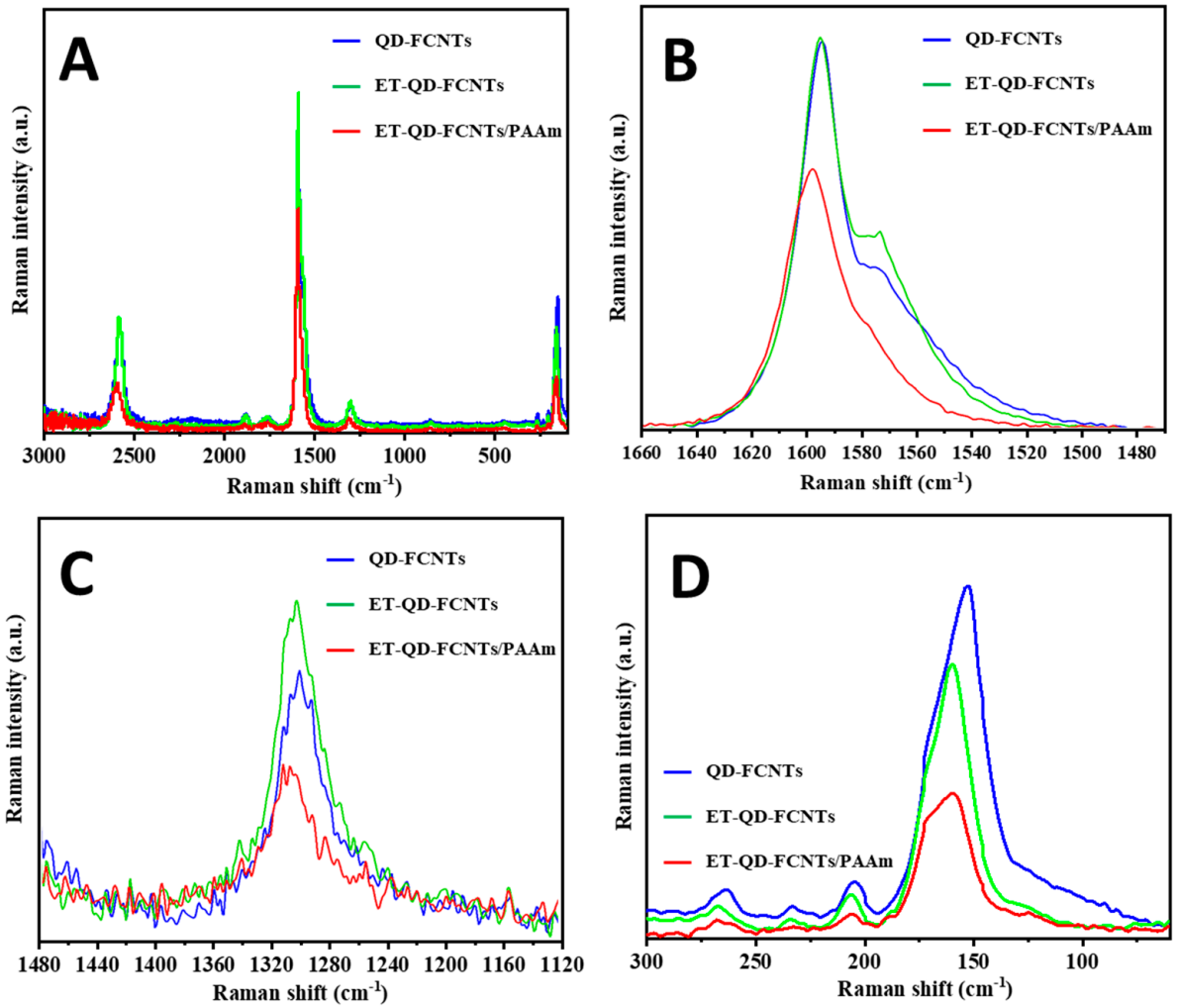

Figure 3. Raman spectra of QD-FCNTs, ET-QD-FCNTs, and ET-QD-FCNT/PAAm microgel composites. (**A**) Full spectra; (**B**) Enlarged G-band area; (**C**) Enlarged D-band area; and (**D**) Enlarged Radial Breathing Mode (RBM) Band area.

To prepare hydrogels used for incorporating with CNTs, we need a low-energy cost synthesis method as well. Synthesizing hydrogels in an aqueous system typically results in uniform, macroscopic hydrogels. However, when using an alcohol system—commonly employed for the precipitation and purification of polyacrylamide polymers, the growth of PAAm microgels is limited. Instead of forming macroscopic networks, the hydrogels synthesized in alcohol remain as microgels, ceasing growth once they reach certain sizes. As shown in Figure 4A, the microgels formed in ethanol are visible as low-density white powders. When these microgels are dispersed in D.I. water using a 360 W ultrasonication probe for 10 min, they produce a cloudy, milky colloidal suspension. The Tyndall effect is clearly observed when a red laser beam passes through the suspension, with the light path being visible from a direction perpendicular to the beam (Figure 4B). This phenomenon confirms the microgel nature of the suspension, indicating that the particles are both small and well-dispersed. Dynamic light scattering (DLS) measurements revealed an average particle size of approximately 0.75 μm, as shown in Figure 4C. The FT-IR spectrum of PAAm microgels (Figure 2B) shows two distinct stretching vibration peaks located at 1610 and 1650 cm^{-1} for amide II and amide I, respectively. Additionally, the peak aroused at 1440 cm^{-1} is attributed to the C-N bond, while the peaks at 3340 and 2938 cm^{-1} are assigned to the N-H and C-H bonds, respectively.

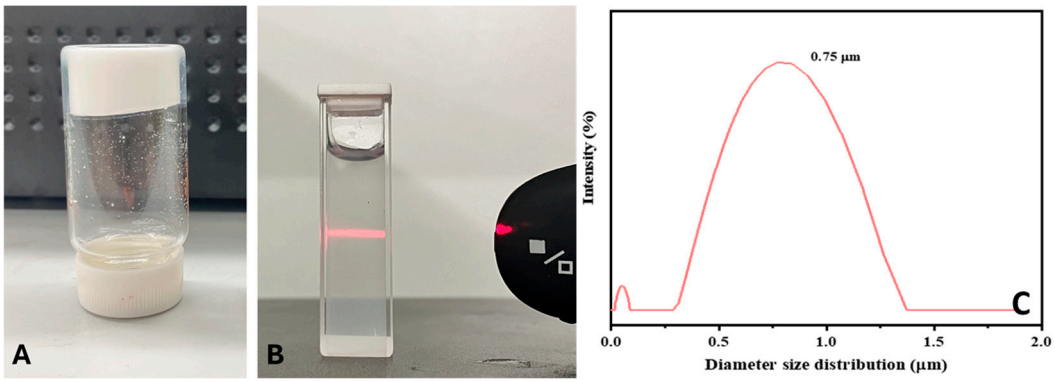

Figure 4. (**A**). As-synthesized PAAm microgel; (**B**). Tyndall effect of the dissolved microgel in D.I. water; (**C**) Dynamic Light Scattering (DLS) size measurement of the microgel.

To prepare the CNTs/microgels composites, a selected amount of dried PAAm microgels was dispersed in deionized water and sonicated together with either QD-FCNTs or ET-QD-FCNTs at a mass ratio of approximately 5% to the dried microgel. The resulting black dispersion was centrifuged to separate the composite materials from the solution. After drying to remove the absorbed water, the composite surfaces, those facing the center of the centrifuge tube and those facing the tube wall, were analyzed using ATR-FTIR, respectively (Figure 5).

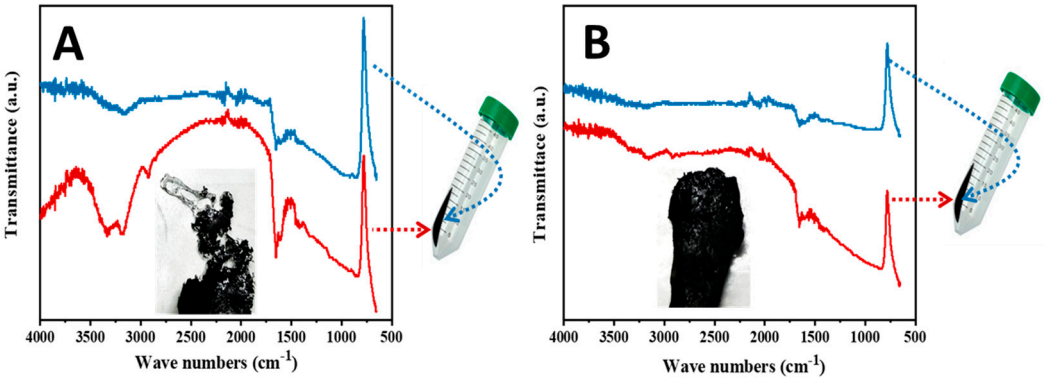

Figure 5. ATR-FTIR analysis of (**A**) QD-FCNT/PAAm and (**B**) ET-QD-FCNT/PAAm microgel composites. Dark red traces: the sample side facing the centrifuge tube wall; Light bl traces: the sample side facing the center of the centrifuge tube.

In the case of the composites without TMPD treatment (QD-FCNTs/PAAm, Figure 5A), the wall-facing side showed more intense PAAm adsorption bands than the center-facing side. This difference could be attributed to the slippage of PAAm microgels from the QD-FCNTs networks under the centrifugal force, or incomplete incorporation of the hydrogel with the QD-FCNTs. By contrast, in the composites made of PAAm microgels and ET-QD-FCNTs, the FTIR adsorption band intensities were nearly identical on both the wall-facing and center-facing sides after centrifugation (Figure 5B). This suggests that the ET-QD-FCNTs enhanced the bonding interaction between the PAAm microgels and the nanotubes, likely due to the additional -OH functional groups formed after TMPD treatment (Scheme 1), resulting in stronger and more stable composites. The centrifugal force was insufficient to separate the microgels and CNTs phases with enhanced interfacial interaction, thus preventing slippage and producing a more stable composite material, as confirmed by the digital photograph inset in Figure 5. The absence of a significant difference between the wall-facing and center-facing sides in the ET-QD-FCNT/PAAm composites after centrifugation indicates a uniform and stable composite structure. This uniformity is crucial for large-scale production, as we anticipate that the enhanced CNT/microgel

interactions provided by the TMPD-treatment can maintain composite consistency across larger volumes, minimizing potential issues related to phase separation or inhomogeneity.

The ET-QD-FCNTs/PAAm microgels composites were further characterized using Raman spectroscopy (Figure 3, red traces). The presence of the microgel diluted the CNT fraction in the sample, leading to a decrease in the peak intensities of the G-band (Figure 3B, red trace), D-band (Figure 3C, red trace), and RBM bands (Figure 3D, red trace). However, all Raman bands exhibited upshifts in band frequency compared to CNT samples without the PAAm microgel (Figure 3, green and blue traces). This upshift is attributed to the compressive strain exerted on the CNTs by the shrinking of the PAAm microgels after the drying process, which leads to a more rigid carbon lattice and increases the vibrational frequencies.

Figure 6 presents the TGA curves for the pure PAAm microgel, QD-FCNTs/PAAm, and ET-QD-FCNTs/PAAm microgel composites. Below 100 °C, all samples exhibit a slight weight loss, attributed to the evaporation of loosely bound or absorbed moisture. Up to 240 °C, the weight loss remains minimal (around 9%) across all samples, demonstrating that the materials are thermally stable within this range. The decomposition of the pure PAAm microgel accelerates at approximately 360 °C, whereas the QD-FCNTs/PAAm and ET-QD-FCNTs/PAAm composites show a delayed onset of decomposition, starting around 460 °C. This indicates that incorporating CNTs significantly enhances the thermal stability of the PAAm microgels. Although both QD-FCNTs/PAAm and ET-QD-FCNTs/PAAm composites exhibit similar decomposition temperatures, the ET-QD-FCNTs/PAAm composite shows a less steep decomposition curve, suggesting a more gradual weight loss compared to the untreated QD-FCNTs/PAAm composite. The steeper decomposition of the untreated QD-FCNTs/PAAm is likely due to insufficient interaction between the QD-FCNTs and the PAAm microgels, which limits the contact area and reduces the thermal stabilization effect provided by the CNTs. Weaker CNT–microgel interactions also result in larger microgel domains that, when decomposed, create larger pores through which volatile components can escape, leading to a faster and more pronounced mass loss. In contrast, the TMPD-treated ET-QD-FCNTs form more uniform interactions with the PAAm microgels via the newly introduced hydroxyl groups. This increases the contact surface area and reduces the size of the microgel domains, which slows down the decomposition process.

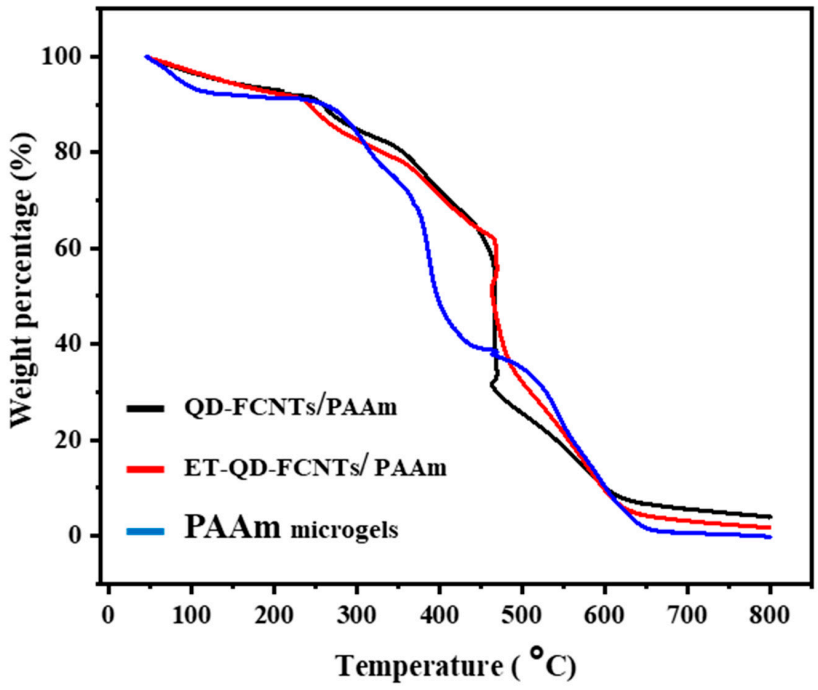

Figure 6. Thermogravimetric analysis (TGA) of PAAm microgels, QD-FCNT/PAAm, and ET-QD-FCNT/PAAm composites in air.

Upon heating to 800 °C, approximately 3.8% of the original weight of the ET-QD-FCNT/PAAm composite and 1.6% of the QD-FCNTs/PAAm composite remain as residues. In contrast, the pure PAAm microgels fully decompose by 700 °C. The lower percentage of residue in the ET-QD-FCNTs/PAAm composite is likely due to the stronger interactions between the CNTs and the polymer, resulting in more uniform dispersion of individual nanotubes. In the case of the untreated QD-FCNTs/PAAm composites, weaker interactions may cause some CNTs to remain bundled, leading to higher residual mass after heating, as the dense nanotubes packing in these bundles reduce the evaporation of volatile components.

To assess the water retention properties, the prepared composites (without drying) were placed in centrifuge tubes inside a ventilated incubator at 35 °C, simulating the warm conditions of agricultural fields. We measured the controlled water release properties of the QD-FCNT/PAAm and ET-QD-FCNT/PAAm microgel composites by tracking the percentage of water evaporation over a period of 350 h. As shown in Figure 7, although both composites initially retained the same amount of water (96.7%), the TMPD-treated ET-QD-FCNT/PAAm microgel composites demonstrated slower water evaporation compared to the untreated QD-FCNT/PAAm composites over 300 h. Specifically, the QD-FCNT/PAAm composites took 142 h to lose 88% of their weight, while the ET-QD-FCNT/PAAm composites required 220 h to reach the same weight loss. This reflects a 55% increase in water retention time, achieved solely through the energy-free surface treatment of the QD-FCNTs with a low dosage of TMPD. This improved water retention is likely due to stronger interactions between the ET-QD-FCNTs and the PAAm microgels, creating a more tightly linked composite structure via the nanotubes, which effectively locks in water for a longer duration.

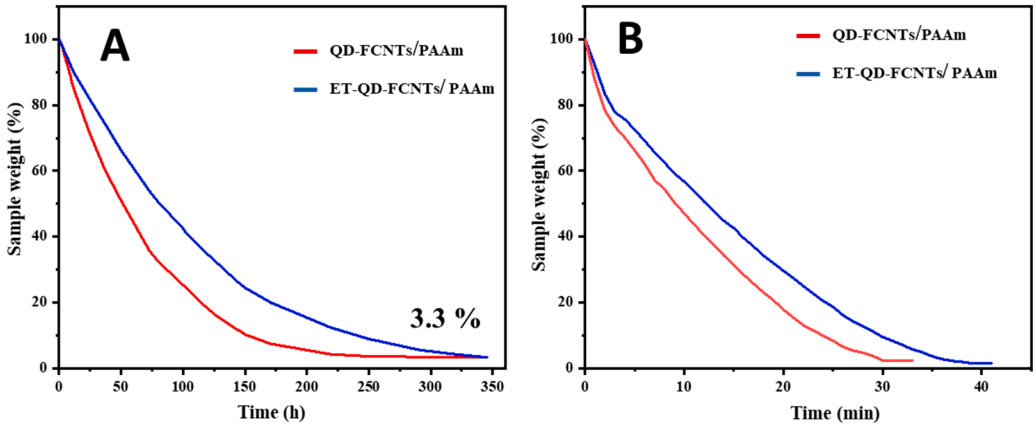

Figure 7. Water retention studies of QD-FCNTs/PAAm and ET-QD-FCNTs/PAAm composites in a (**A**) 35 °C incubator and (**B**) 80 °C moisture analyzer.

To further confirm the water retention properties, we conducted a rapid de-moisture analysis of the samples at 80 °C using a moisture analyzer. As shown in Figure 7B, de-moisture at 80 °C was completed for QD-FCNT/PAAm composites within approximately 30 min, while the same process for ET-QD-FCNT/PAAm composites took around 40 min. This also indicates improved water retention time for the ET-QD-FCNT/PAAm composites compared to those made with untreated QD-FCNTs, suggesting enhanced water/composite interactions even at elevated temperatures. Notably, at 80 °C, the remaining weight percentage after complete water release was 97.6% for the QD-FCNT/PAAm microgel composites and 98.5% for the ET-QD-FCNT/PAAm microgel composites. The water losses were slightly higher than those in the water release tests at 35 °C because of the higher drying temperature.

Notably, these composites require only a small fraction of CNTs to achieve the above exceptional functions. We conducted a composition analysis of the ET-QD-FCNTs/PAAm composites fully saturated with water, based on the initially added components and the

amount of water lost after complete drying. As shown in Figure 8, water constitutes 98.5% of the composite, PAAm accounts for 1.4%, and the ET-QD-FCNTs represent just around 0.1%, demonstrating the exceptional performance of ET-QD-FCNTs as an efficient microgel additive. These results highlight the effectiveness of the ET-QD-FCNT/PAAm microgel composite in maintaining water retention under thermal stress, underscoring its potential for applications in water management and sustained release environments. Regarding the potential fluorine release and environmental impact, the trace amounts of fluorine still detected after treatment with TMPD suggest that the remaining fluorine atoms are strongly bonded within the carbon nanotube lattice as stable C–F bonds. These bonds are chemically inert and unlikely to leach into the environment under normal conditions. Moreover, the incorporation of ET-QD-FCNTs into the PAAm microgel matrix provides additional physical encapsulation, further minimizing the potential for fluorine release. Therefore, the ET-QD-FCNTs/PAAm composites are expected to be environmentally safe for agricultural applications.

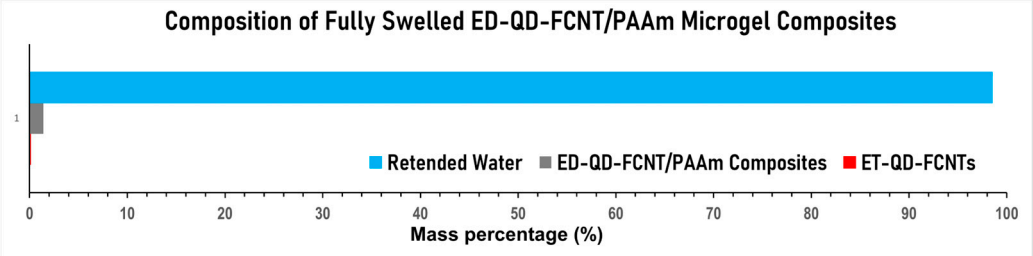

Figure 8. Composition analysis of ET-QD-FCNT/PAAm composites after complete drying.

To provide a clear comparison of our eco-friendly modification method with other conventional techniques, we have summarized the advantages and possible limitations of this work in Table 2 below:

Table 2. Advantages and Possible Limitations of Current Work.

Aspects	Advantages	Limitations
Eco-Friendly Treating QD-FCNT with TMPD	1. Utilizes a mild, near zero-energy process 2. Avoids the use of large amounts of harsh chemicals like concentrated acids or piranha solutions 3. Reduces environmental impact and hazardous waste 4. Enhances hydrophilicity of CNTs by introducing hydroxyl groups 5. Improves compatibility with PAAm microgels	Increase in oxygen content is not very high (but is sufficient to enhance CNT–microgel interaction)
Composite Performance	6. Retains over 30 times of its own weight in water 7. After the eco-friendly surface treatment of QD-FCNTs, the ET-QD-FCNT composite achieves a 55% increase in water retention time at 35 °C 8. Enhances thermal stability of composites (according to TGA) 9. Ensures homogeneous dispersion of microgels on CNT surfaces	The water-retention improvement may be sufficient for agricultural applications but may not meet the requirements of applications needing extremely high water-retention. (e.g., diapers)

Table 2. *Cont.*

Aspects	Advantages	Limitations
Cost-Effectiveness	10. Reduces energy and chemical costs due to mild treatment conditions 11. Utilizes quality-downgraded materials, adding value to waste 12. Low ecological footprint due to reduced chemical and energy usage 13. Supports sustainable material practices and circular economy principles	Although our method for reusing QD-FCNTs is cost-effective, the initial fabrication of FCNTs (before quality degradation) is expensive.

4. Conclusions

This research successfully demonstrated the repurposing of quality-downgraded fluorinated carbon nanotubes (QD-FCNTs) as eco-friendly nano-additives in polyacrylamide (PAAm) microgel composites for water retention applications. The study highlights how QD-FCNTs, degraded through long-term storage, can be re-functionalized using a mild, low-dosage treatment with organic electron donors. This process enhances the hydrophilicity of the CNT surfaces by introducing small amounts of hydroxyl groups at defect sites, significantly improving their compatibility and interaction with PAAm microgels. The treatment results in ET-QD-FCNT/PAAm composites that are more thermally stable and exhibit a 55% increase in water retention time compared to untreated QD-FCNT/PAAm composites. These improvements underscore the critical role of CNT surface functionalization in achieving enhanced composite performance. Importantly, these composites achieved this performance with just 0.1% reused CNT loading, highlighting their cost-efficiency and environmental sustainability. For future research, we suggest exploring the scalability of this eco-friendly surface treatment for industrial applications, ensuring that the process remains cost-effective and environmentally friendly at larger production scales. Investigating the long-term environmental impact and degradability of these composites in agricultural settings is also crucial to assessing their sustainability and safety over extended use. Additionally, optimizing the QD-FCNT/PAAm composites may be necessary for applications that require exceptionally high water retention rates.

To summarize, this study offers an innovative approach to re-functionalize and repurpose QD-FCNTs for environmentally friendly applications. By utilizing a low-energy, sustainable treatment, the approach extends the lifecycle of high-value CNT-based materials, contributing to the circular economy. The findings provide practical solutions for improving water retention, making this method potentially applicable to sustainable agriculture and other environment-focused applications.

Author Contributions: Conceptualization, Y.G.; methodology, Y.G.; material synthesis, F.L.E., P.U.O. and M.T.I.; characterization, F.L.E., Y.G., T.G., P.U.O. and M.T.I.; data analysis, Y.G. and G.P.O.; writing—original draft preparation, Y.G., G.P.O. and P.U.O.; supervision, Y.G.; project administration, Y.G.; funding acquisition, Y.G. All authors have read and agreed to the published version of the manuscript.

Funding: This research was funded by the USDA National Institute of Food and Agriculture (USDA-NIFA)'s 1890 Land Grant Institution Capacity Building Grants (CBG) Program, grant number 2022-38821-37305. Any opinions, findings, conclusions, or recommendations expressed in this material are those of the authors and do not necessarily reflect the views of the USDA-NIFA.

Data Availability Statement: The data are available from the corresponding author upon reasonable request.

Conflicts of Interest: The authors declare no conflict of interest. The funders had no role in the design of the study; in the collection, analyses, or interpretation of data; in the writing of the manuscript; or in the decision to publish the results.

References

1. Ramasubramanian, B.; Ling, J.; Jose, R.; Ramakrishna, S. Ten major challenges for sustainable lithium-ion batteries. *Cell Rep. Phys. Sci.* **2024**, *5*, 102032. [CrossRef]
2. Amarasekara, A.S.; Shrestha, A.B. Facile recovery of lithium as Li_2CO_3 or Li_2O from α-hydroxy-carboxylic acid chelates through pyrolysis and the decomposition mechanism. *J. Anal. Appl. Pyrolysis* **2024**, *179*, 106471. [CrossRef]
3. Amarasekara, A.S.; Wang, D.; Shrestha, A.B. Efficient leaching of metal ions from spent Li-ion battery combined electrode coatings using hydroxy acid mixtures and regeneration of lithium nickel manganese cobalt oxide. *Batteries* **2024**, *10*, 170. [CrossRef]
4. Mishra, G.; Jha, R.; Meshram, A.; Singh, K.K. A review on recycling of lithium-ion batteries to recover critical metals. *J. Environ. Chem. Eng.* **2022**, *10*, 108534. [CrossRef]
5. Jha, M.K.; Kumari, A.; Jha, A.K.; Kumar, V.; Hait, J.; Pandey, B.D. Recovery of lithium and cobalt from waste lithium ion batteries of mobile phone. *Waste Manag.* **2013**, *33*, 1890–1897. [CrossRef] [PubMed]
6. Niu, B.; Xu, Z.; Xiao, J.; Qin, Y. Recycling hazardous and valuable electrolyte in spent lithium-ion batteries: Urgency, progress, challenge, and viable approach. *Chem. Rev.* **2023**, *123*, 8718–8735. [CrossRef]
7. Mao, Z.; Song, Y.; Zhen, A.G.; Sun, W. Recycling of electrolyte from spent lithium-ion batteries. *Next Sustain.* **2024**, *3*, 100015. [CrossRef]
8. Qiu, X.; Wang, C.; Xie, L.; Zhu, L.; Cao, X.; Ji, X. Challenges and perspectives towards direct regeneration of spent $LiFePO_4$ cathode. *J. Power Sources* **2024**, *602*, 234365. [CrossRef]
9. Zhu, H.; Chen, S.; Yao, X.; Yang, K.; Zhao, W.; Chen, T.; Yang, L.; Pan, F. Upcycling spent cathode materials to bifunctional catalysts for high-stability lithium–sulfur batteries. *Adv. Funct. Mater.* **2024**, *34*, 2401470. [CrossRef]
10. Arshad, F.; Li, L.; Amin, K.; Fan, E.; Manurkar, N.; Ahmad, A.; Yang, J.; Wu, F.; Chen, R. A comprehensive review of the advancement in recycling the anode and electrolyte from spent lithium ion batteries. *ACS Sustain. Chem. Eng.* **2020**, *8*, 13527–13554. [CrossRef]
11. Wang, Y.; Lv, X.; Kimura, H.; Yang, Y.; Hou, C.; Xie, X.; Sun, X.; Zhang, Y.; Du, W.; Yang, X. Recycling of graphite anode from retired lithium-ion batteries to cathode of high-performance lithium-oxygen batteries. *J. Energy Storage* **2024**, *89*, 111540. [CrossRef]
12. Liu, Y.; Gao, Y.; Altalhi, T.; Liu, D.-J.; Yakobson, B.I. A quantum mechanical MP2 study of the electronic effect of nonplanarity on the carbon pyramidalization of fullerene C_{60}. *Nanomaterials* **2024**, *14*, 1576. [CrossRef] [PubMed]
13. Maheswaran, R.; Shanmugavel, B.P. A critical review of the role of carbon nanotubes in the progress of next-generation electronic applications. *J. Electron. Mater.* **2022**, *51*, 2786–2800. [CrossRef] [PubMed]
14. Jiang, Z.; Zhao, Y.; Lu, X.; Xie, J. Fullerenes for rechargeable battery applications: Recent developments and future perspectives. *J. Energy Chem.* **2021**, *55*, 70–79. [CrossRef]
15. Fang, R.; Chen, K.; Yin, L.; Sun, Z.; Li, F.; Cheng, H.-M. The regulating role of carbon nanotubes and graphene in lithium-ion and lithium–sulfur batteries. *Adv. Mater.* **2019**, *31*, 1800863. [CrossRef] [PubMed]
16. Yu, X.; Liu, D.; Kang, L.; Yang, Y.; Zhang, X.; Lv, Q.; Qiu, S.; Jin, H.; Song, Q.; Zhang, J.; et al. Recycling strategy for fabricating low-cost and high-performance carbon nanotube TFT devices. *ACS Appl. Mater. Interfaces* **2017**, *9*, 15719–15726. [CrossRef] [PubMed]
17. Schauerman, C.M.; Ganter, M.J.; Gaustad, G.; Babbitt, C.W.; Raffaelle, R.P.; Landi, B.J. Recycling single-wall carbon nanotube anodes from lithium ion batteries. *J. Mater. Chem.* **2012**, *22*, 12008–12015. [CrossRef]
18. Mikhalchan, A.; Ramos Lozano, S.; Fernández Gorgojo, A.; González, C.; Vilatela, J.J. Network structure enabling re-use and near full property retention in CNT sheets recycled from thermoset composites. *Carbon* **2024**, *220*, 118851. [CrossRef]
19. Wang, H.; Chen, Y.; Yu, H.; Liu, W.; Kuang, G.; Mei, L.; Wu, Z.; Wei, W.; Ji, X.; Qu, B.; et al. A multifunctional artificial interphase with fluorine-doped amorphous carbon layer for ultra-stable Zn anode. *Adv. Funct. Mater.* **2022**, *32*, 2205600. [CrossRef]
20. Wang, T.; Zang, X.; Wang, X.; Gu, X.; Shao, Q.; Cao, N. Recent advances in fluorine-doped/fluorinated carbon-based materials for supercapacitors. *Energy Storage Mater.* **2020**, *30*, 367–384. [CrossRef]
21. Huang, Y.; Zhang, W.; Bai, M.; Huang, X. One-pot fabrication of magnetic fluorinated carbon nanotubes adsorbent for efficient extraction of perfluoroalkyl carboxylic acids and perfluoroalkyl sulfonic acids in environmental water samples. *Chem. Eng. J.* **2020**, *380*, 122392. [CrossRef]
22. Kinloch, I.A.; Suhr, J.; Lou, J.; Young, R.J.; Ajayan, P.M. Composites with carbon nanotubes and graphene: An outlook. *Science* **2018**, *362*, 547–553. [CrossRef] [PubMed]
23. Van Tran, V.; Wi, E.; Shin, S.Y.; Lee, D.; Kim, Y.A.; Ma, B.C.; Chang, M. Microgels based on 0D-3D carbon materials: Synthetic techniques, properties, applications, and challenges. *Chemosphere* **2022**, *307*, 135981. [CrossRef] [PubMed]
24. Hu, X.-G.; Hou, P.-X.; Wu, J.-B.; Li, X.; Luan, J.; Liu, C.; Liu, G.; Cheng, H.-M. High-efficiency and stable silicon heterojunction solar cells with lightly fluorinated single-wall carbon nanotube films. *Nano Energy* **2020**, *69*, 104442. [CrossRef]
25. Mohammed, M.K.A.; Al-Mousoi, A.K.; Kumar, A.; Katae, A.R.J.; Khaleel, O.A.; Ahmed, D.S.; Hossain, M.K. Fluorinated carbon nanotubes: A low-cost hole transport layer for perovskite solar cells. *J. Mater. Sci.* **2023**, *58*, 11748–11760. [CrossRef]
26. Liu, W.; Deng, N.; Wang, G.; Yu, R.; Wang, X.; Cheng, B.; Ju, J.; Kang, W. Fluoridation routes, function mechanism and application of fluorinated/fluorine-doped nanocarbon-based materials for various batteries: A review. *J. Energy Chem.* **2023**, *85*, 363–393. [CrossRef]

27. Zhang, G.; Colin, M.; Yang, X.; Sun, S.; Dodelet, J.-P.; Dubois, M. CF bonding in fluorinated N-doped carbons. *Appl. Surf. Sci.* **2022**, *577*, 151721. [CrossRef]
28. Wang, W.; Lu, X.; Su, P.; Li, Y.; Cai, J.; Zhang, Q.; Zhou, M.; Arotiba, O. Enhancement of hydrogen peroxide production by electrochemical reduction of oxygen on carbon nanotubes modified with fluorine. *Chemosphere* **2020**, *259*, 127423. [CrossRef]
29. Wang, Y.; He, T.; Cheng, Z.; Liu, M.; Ji, J.; Chang, X.; Xu, Q.; Liu, Y.; Liu, X.; Qin, J. Mechanically strong and tough polyimide aerogels cross-linked with amine functionalized carbon nanotubes synthesized by fluorine displacement reaction. *Compos. Sci. Technol.* **2020**, *195*, 108204. [CrossRef]
30. Li, Y.; Wu, X.; Liu, C.; Wang, S.; Zhou, P.; Zhou, T.; Miao, Z.; Xing, W.; Zhuo, S.; Zhou, J. Fluorinated multi-walled carbon nanotubes as cathode materials of lithium and sodium primary batteries: Effect of graphitization of carbon nanotubes. *J. Mater. Chem. A* **2019**, *7*, 7128–7137. [CrossRef]
31. Xue, D.; Zhu, D.; Xiong, W.; Cao, T.; Wang, Z.; Lv, Y.; Li, L.; Liu, M.; Gan, L. Template-free, self-doped approach to porous carbon spheres with high N/O contents for high-performance supercapacitors. *ACS Sustain. Chem. Eng.* **2019**, *7*, 7024–7034. [CrossRef]
32. Yue, H.; Zhang, W.; Liu, H.; Liu, Z.; Zhong, G.; Yang, Y. Synthesis and characterization of fluorinated carbon nanotubes for lithium primary batteries with high power density. *Nanotechnology* **2013**, *24*, 424003. [CrossRef] [PubMed]
33. Liu, X.; Kumar, P.V.; Chen, Q.; Zhao, L.; Ye, F.; Ma, X.; Liu, D.; Chen, X.; Dai, L.; Hu, C. Carbon nanotubes with fluorine-rich surface as metal-free electrocatalyst for effective synthesis of urea from nitrate and CO_2. *Appl. Catal. B Environ.* **2022**, *316*, 121618. [CrossRef]
34. Han, S.-G.; Ma, D.-D.; Zhou, S.-H.; Zhang, K.; Wei, W.-B.; Du, Y.; Wu, X.-T.; Xu, Q.; Zou, R.; Zhu, Q.-L. Fluorine-tuned single-atom catalysts with dense surface Ni-N_4 sites on ultrathin carbon nanosheets for efficient CO_2 electroreduction. *Appl. Catal. B Environ.* **2021**, *283*, 119591. [CrossRef]
35. Chang, Y.; Chen, J.; Jia, J.; Hu, X.; Yang, H.; Jia, M.; Wen, Z. The fluorine-doped and defects engineered carbon nanosheets as advanced electrocatalysts for oxygen electroreduction. *Appl. Catal. B Environ.* **2021**, *284*, 119721. [CrossRef]
36. Kharitonov, A.P.; Tkachev, A.G.; Blohin, A.N.; Dyachkova, T.P.; Kobzev, D.E.; Maksimkin, A.V.; Mostovoy, A.S.; Alekseiko, L.N. Reinforcement of bisphenol-F epoxy resin composites with fluorinated carbon nanotubes. *Compos. Sci. Technol.* **2016**, *134*, 161–167. [CrossRef]
37. Gao, Y.; Chen, H.; Ge, J.; Zhao, J.; Li, Q.; Tang, J.; Cui, Y.; Chen, L. Direct intertube cross-linking of carbon nanotubes at room temperature. *Nano Lett.* **2016**, *16*, 6541–6547. [CrossRef]
38. Gao, Y.; Islam, M.T.; Otuokere, P.U.; Pulikkathara, M.; Liu, Y. The stability of UV-defluorination-driven crosslinked carbon nanotubes: A Raman study. *Nanomaterials* **2024**, *14*, 1464. [CrossRef]
39. Datsyuk, V.; Kalyva, M.; Papagelis, K.; Parthenios, J.; Tasis, D.; Siokou, A.; Kallitsis, I.; Galiotis, C. Chemical oxidation of multiwalled carbon nanotubes. *Carbon* **2008**, *46*, 833–840. [CrossRef]
40. Bulusheva, L.G.; Fedoseeva, Y.V.; Okotrub, A.V.; Flahaut, E.; Asanov, I.P.; Koroteev, V.O.; Yaya, A.; Ewels, C.P.; Chuvilin, A.L.; Felten, A.; et al. Stability of fluorinated double-walled carbon nanotubes produced by different fluorination techniques. *Chem. Mater.* **2010**, *22*, 4197–4203. [CrossRef]
41. Mickelson, E.T.; Huffman, C.B.; Rinzler, A.G.; Smalley, R.E.; Hauge, R.H.; Margrave, J.L. Fluorination of single-wall carbon nanotubes. *Chem. Phys. Lett.* **1998**, *296*, 188–194. [CrossRef]
42. Gao, Y.; Zhang, L.; Xia, Z.; Li, C.M.; Dai, L. Hole-punching for enhancing electrocatalytic activities of 2D graphene electrodes: Less is more. *J. Chem. Phys.* **2020**, *153*, 074701. [CrossRef] [PubMed]
43. Bettinger, H.F. The reactivity of defects at the sidewalls of single-walled carbon nanotubes: The Stone-Wales defect. *J. Phys. Chem. B* **2005**, *109*, 6922–6924. [CrossRef]
44. Li, L.X.; Li, F. The effect of carbonyl, carboxyl and hydroxyl groups on the capacitance of carbon nanotubes. *New Carbon Mater.* **2011**, *26*, 224–228. [CrossRef]
45. Battie, Y.; Dossot, M.; Allali, N.; Mamane, V.; Naciri, A.E.; Broch, L.; Soldatov, A.V. Mild covalent functionalization of single-walled carbon nanotubes highlighted by spectroscopic ellipsometry. *Carbon* **2016**, *96*, 557–564. [CrossRef]
46. Imran, M.; Raza, M.; Noor, H.; Faraz, S.M.; Raza, A.; Farooq, U.; Khan, M.E.; Ali, S.K.; Bakather, O.Y.; Ali, W.; et al. Insight into mechanism of excellent visible-light photocatalytic activity of CuO/MgO/ZnO nanocomposite for advanced solution of environmental remediation. *Chemosphere* **2024**, *359*, 142224. [CrossRef]
47. Raza, M.; Farooq, U.; Khan, M.E.; Naseem, K.; Alam, S.; Khan, M.Y.; Ali, W.; Ali, S.K.; Bakather, O.Y.; Zoubi, W.A.; et al. Development of simplistic and stable Co-doped ZnS nanocomposite towards excellent removal of bisphenol A from wastewater and hydrogen production: Evaluation of reaction parameters by response surface methodology. *J. Taiwan Inst. Chem. Eng.* **2024**, *163*, 105654. [CrossRef]
48. Saito, R.; Hofmann, M.; Dresselhaus, G.; Jorio, A.; Dresselhaus, M.S. Raman spectroscopy of graphene and carbon nanotubes. *Adv. Phys.* **2011**, *60*, 413–550. [CrossRef]
49. Park, Y.; Hembram, K.P.S.S.; Yoo, R.; Jang, B.; Lee, W.; Lee, S.-G.; Kim, J.-G.; Kim, Y.-I.; Moon, D.J.; Lee, J.-K.; et al. Reinterpretation of single-wall carbon nanotubes by Raman spectroscopy. *J. Phys. Chem. C* **2019**, *123*, 14003–14009. [CrossRef]
50. Telg, H.; Duque, J.G.; Staiger, M.; Tu, X.; Hennrich, F.; Kappes, M.M.; Zheng, M.; Maultzsch, J.; Thomsen, C.; Doorn, S.K. Chiral index dependence of the G^+ and G^- Raman modes in semiconducting carbon nanotubes. *ACS Nano* **2012**, *6*, 904–911. [CrossRef]

51. Jorio, A.; Saito, R.; Hafner, J.H.; Lieber, C.M.; Hunter, M.; McClure, T.; Dresselhaus, G.; Dresselhaus, M.S. Structural (n, m) determination of isolated single-wall carbon nanotubes by resonant Raman scattering. *Phys. Rev. Lett.* **2001**, *86*, 1118–1121. [CrossRef] [PubMed]
52. Tian, Y.; Jiang, H.; Laiho, P.; Kauppinen, E.I. Validity of measuring metallic and semiconducting single-walled carbon nanotube fractions by quantitative Raman spectroscopy. *Anal. Chem.* **2018**, *90*, 2517–2525. [CrossRef] [PubMed]
53. Pehrsson, P.E.; Zhao, W.; Baldwin, J.W.; Song, C.; Liu, J.; Kooi, S.; Zheng, B. Thermal fluorination and annealing of single-wall carbon nanotubes. *J. Phys. Chem. B* **2003**, *107*, 5690–5695. [CrossRef]
54. Li, X.-Q.; Hou, P.-X.; Liu, C.; Cheng, H.-M. Preparation of metallic single-wall carbon nanotubes. *Carbon* **2019**, *147*, 187–198. [CrossRef]
55. Shukla, P.K.; Mishra, P.C. Effects of diameter, length, chirality and defects on the scavenging action of single-walled carbon nanotubes for OH radicals: A quantum computational study. *Chem. Phys.* **2010**, *369*, 101–107. [CrossRef]

Disclaimer/Publisher's Note: The statements, opinions and data contained in all publications are solely those of the individual author(s) and contributor(s) and not of MDPI and/or the editor(s). MDPI and/or the editor(s) disclaim responsibility for any injury to people or property resulting from any ideas, methods, instructions or products referred to in the content.